Biophysical Journal
Article

Biophysical Society

Lipid-Bilayer Dynamics Probed by a Carbon Dot-Phospholipid Conjugate

Sukhendu Nandi,[1] Ravit Malishev,[1] Susanta Kumar Bhunia,[1] Sofiya Kolusheva,[2] Jürgen Jopp,[2] and Raz Jelinek[1,2,*]

[1]Department of Chemistry and [2]Ilse Katz Institute for Nanoscale Science & Technology, Ben Gurion University of the Negev, Beer Sheva, Israel

ABSTRACT Elucidating the dynamic properties of membranes is important for understanding fundamental cellular processes and for shedding light on the interactions of proteins, drugs, and viruses with the cell surface. Dynamic studies of lipid bilayers have been constrained, however, by the relatively small number of pertinent molecular probes and the limited physicochemical properties of the probes. We show that a lipid conjugate comprised of a fluorescent carbon dot (C-dot) covalently attached to a phospholipid constitutes a versatile and effective vehicle for studying bilayer dynamics. The C-dot-modified phospholipids readily incorporated within biomimetic membranes, including solid-supported bilayers and small and giant vesicles, and inserted into actual cellular membranes. We employed the C-dot-phospholipid probe to elucidate the effects of polymyxin-B (a cytolytic peptide), valproic acid (a lipophilic drug), and amyloid-β (a peptide associated with Alzheimer's disease) upon bilayer fluidity and lipid dynamics through the application of various biophysical techniques.

INTRODUCTION

The dynamical properties of membranes, including bilayer fluidity, lipid mobility, and molecular diffusion in membranes, are fundamental determinants of cell membrane functionality (1–4). Modulation of membrane dynamical properties by membrane-active molecules contributes to various important cellular processes, such as cell signaling, biomolecular recognition, and drug uptake (2,4–7). Different bioanalytical techniques, primarily utilizing fluorescent dyes, have been developed to elucidate the dynamical parameters of membranes and have been applied both in biomimetic systems (e.g., vesicles) and in actual cell systems (1,2,8–11). Many membrane-dynamics probes, however, exhibit limitations such as inefficient insertion into lipid bilayers, disruption of bilayer organization, low fluorescence brightness, rapid photobleaching, and constraints in terms of excitation/emission wavelengths.

Carbon dots (C-dots), recently developed fluorescent carbonaceous nanoparticles, have attracted significant interest due to their unique structural and photophysical properties (12–20). C-dots are chemically stable and provide a broad excitation/emission spectral range and low photobleaching, making them promising conduits for biological imaging applications (12,21–23). Furthermore, C-dots can be produced from a wide variety of natural carbon sources, providing a means for modulating their structural properties and underscoring their potentially better biocompatibility compared with inorganic nanoparticles utilized for cellular investigations, such as quantum dots (24,25). We recently synthesized amphiphilic C-dots and demonstrated their use in membrane- and cell-imaging applications (26).

Here, we show that phospholipids covalently coupled to C-dots at the phosphate residue constitute a versatile and sensitive vehicle for studying lipid dynamics in membranes. The new, to our knowledge, phospholipid conjugate retains the unique fluorescence properties of the C-dots, specifically the broad excitation/emission range (e.g., multicolor luminescence), brightness, and sensitivity to molecular environments, and can be readily incorporated within membrane bilayers. We applied various fluorescence-based techniques to analyze membrane dynamical properties, particularly modulation of lipid mobility induced by prominent membrane-active compounds.

MATERIALS AND METHODS

Materials

All solvents used in this work were high-performance liquid chromatography (HPLC) grade and were used directly unless noted otherwise.

Submitted December 30, 2015, and accepted for publication April 4, 2016.

*Correspondence: razj@bgu.ac.il

Editor: Joseph Falke.

http://dx.doi.org/10.1016/j.bpj.2016.04.005

1,2-Dimyristoyl-*sn*-glycero-3-phosphocholine (DMPC), 1,2-dioleoyl-*sn*-glycero-3-phosphocholine (DOPC), cholesterol (ovine wool, >98%), and 1,2-dimyristoyl-*sn*-glycero-3-phosphoethanolamine-N-(7-nitro-2-1,3-benzoxadiazol-4-yl) (N-NBD-PE) were obtained from Avanti Polar Lipids ((Alabaster, AL). Amyloid $\beta_{1\text{-}40}$ ($A\beta_{1\text{-}40}$) was purchased from Peptron (Daejeon, South Korea) in a lyophilized form at >90% purity (HPLC). 1,1,1,3,3,3-Hexafluoro-2-propanol and sodium phosphate monobasic were purchased from Sigma-Aldrich (Rehovot, Israel).

$A\beta_{1\text{-}40}$ sample preparation

$A\beta_{1\text{-}40}$ was dissolved in 1,1,1,3,3,3-hexafluoroisopropanol (HFIP) at a concentration of 1 mg/mL and stored at −20°C until use to prevent fibril formation. For each experiment, the solution was thawed, and the required amount was dried by evaporation for 6−7 h to remove the HFIP. The dried peptide samples were dissolved in buffer consisting of 10 mM NaH_2PO_4, pH 7.4, at room temperature.

Synthesis of C-dot-DMPC

For synthesis of (3*R*,4*R*)-2,5-dioxotetrahydrofuran-3,4-diyl didodecanoate (compound 1; Fig. S1 in the Supporting Material), 30 g of finely powdered *L*-tartaric acid (0.2 mol) and 166 mL of lauroyl chloride (0.7 mol) were put into a 500 mL round bottom flask equipped with a magnetic stirrer bar and an air bubbler. The reaction mixture was heated for 24 h at 90°C and then cooled to room temperature. The lauric acid and excess lauroyl chloride were removed by dissolving the crude mixture in a minimum amount of *n*-hexane and kept at room temperature for 12 h. The product was precipitated in *n*-hexane, which was subsequently filtered, washed thoroughly with *n*-hexane, and dried under vacuum to obtain 89 g of compound 1 (yield: 90%) as white powder.

For synthesis of (2*R*,3*R*)-2,3-Bis(dodecanoyloxy)-4-oxo-4-(((2*R*,3*S*,4*S*,5*R*)-3,4,5,6-tetrahydroxytetrahydro-2H-pyran-2-yl)methoxy)butanoic acid (compound 2; Fig. S1), compound 1 (11 g, 0.022 mol) was added to a solution of *D*-glucose (20 g, 0.11 mol) in 150 mL anhydrous dimethylformamide (DMF) with stirring under argon and the reaction mixture was allowed to cool down to 0°C, followed by addition of absolute dry pyridine (1.8 mL, 0.022 mol). The reaction was allowed to continue under an argon atmosphere at 0°C for 2–3 h, followed by an additional 3 days at room temperature. After completion of the reaction, the mixture was poured into an ice-water mixture and then 2 N HCl was added at 0°C with vigorous stirring. The product was extracted with ethyl acetate and the extracted ethyl acetate layer was washed four times with brine solution and dried over sodium sulfate. The ethyl acetate was then removed under reduced pressure to obtain the crude product (12.5 g, 83%). The crude product contained a mixture of regio-isomers (monoesters) of *D*-glucose (as confirmed by thin-layer chromatography (TLC), HPLC-MS, and ^{13}C NMR). From the crude product, the 6-substituted monoester (compound 2) was precipitated in the following manner: the crude mixture was dissolved in a minimum amount of n-hexane under reflux and a half volume of acetone was added. The solution was cooled to 0°C in an ice-water bath and then kept for 12 h at room temperature. Compound 2 was precipitated from the mixture, which was then filtered and dried to obtain 3.1 g (21%, $\alpha/\beta = 1.8/1$) of compound 2 as a mixture of anomers.

For synthesis and characterization of C-dots (compound 3; Fig. S1), 100 mg of compound 2 and 330 μL of deionized water were placed in a Teflon-film-tightened, septum-capped test tube and then heated in an oven to 125°C for 2.5 h. Upon completion of the hydrothermal reaction, the resultant mixture was allowed to cool to room temperature, yielding a brown precipitate implying the formation of C-dots. The brown precipitate was then redispersed in 5 mL of chloroform through vortexing and centrifuged at 14,000 rpm for 30 min to remove high-weight precipitate and agglomerated particles. Chloroform was gently evaporated under reduced pressure to obtain a brown solid. The same procedure was repeated with 5 mL acetone, followed by solvent removal under reduced pressure to obtain monodisperse C-dots (compound 3) with a yield of 63 mg.

For synthesis of DMPC-conjugated C-dot (C-dot-DMPC, compound 4; Fig. S1), 50 mg (0.063 mmol) of DMPC was dissolved in degassed dichloromethane (DCM) (10 mL) in a Schlenk flask, followed by addition of 27.2 μL (0.31 mmol) of oxalyl chloride and a catalytic amount of DMF under argon atmosphere. The reaction was continued at room temperature for 12 h under an argon atmosphere. The excess oxalic chloride was removed from the mixture under reduced pressure and the crude reaction mixture was again immediately resuspended in dry degassed DCM, followed by addition of a 5 mL solution of 40 mg of C-dots (compound 3) in DCM and 25.6 μL (0.31 mmol) of absolute dry pyridine, respectively. The reaction was allowed to continue at room temperature for 24 h. The reaction was monitored by TLC by eluting the reaction mixture with methanol and chloroform mixture (1:1, v/v). Perchloric acid in an acetone water mixture, an ammonium molybdate solution in a concentrated nitric acid and water mixture, and an Sn(II) chloride solution in water were used for phosphate detection in TLC. After completion of the reaction, the crude product was concentrated by evaporation under reduced pressure. Ice-cooled doubly-distilled water (DDW) was added to the reaction mixture and then 1 M HCl was added to neutralize pyridine, followed by extraction with DCM. The extracted DCM layer was washed four times with brine solution and dried over sodium sulfate, and the organic layer was removed under reduced pressure to obtain pure C-dot-DMPC with a yield of ~50 mg.

Formation of giant vesicles comprised of DOPC phospholipids and C-dot-DMPC

Giant vesicles (GVs) were prepared by means of a rapid evaporation technique (27). In brief, 2 mg of C-dot-DMPC was dissolved in 500 μL of chloroform by vortexing and sonication, and subsequently added into a 4 mL vial containing 97.5 μL of prepared DOPC stock solution (concentration 25.5 mM) in chloroform. The mixture was then transferred to a 250 mL round-bottom flask and the aqueous phase (2.5 mL of 0.1 M sucrose, 0.1 mM KCl, 50 mM Tris solution, pH 7.4) was carefully added with a pipette and gently stirred for 5 min. The organic solvent was removed in a rotary evaporator under reduced pressure (final pressure 20 mbar) at room temperature. After evaporation for ~4–5 min, an opalescent fluid was obtained with a volume of ~2.5 mL. Then, 200 μL of this fluid was transferred to 35-mm coverglass-bottom confocal dishes (SPL Life Sciences, Seoul, Korea) for fluorescence recovery after photobleaching (FRAP) studies.

Cell membrane labeled with C-dot-DMPC

HeLa cells were cultured on a coverglass-bottom dish with Dulbecco's modified Eagle's medium. After 24 h, 50 μL of a freshly prepared solution of 2 mg C-dot-DMPC or only DMPC in DMSO together with 200 μL of fresh medium was added to the dish and the cells were incubated for 30 min. The cells were then washed with phosphate-buffered saline to remove unbound C-dot-DMPC and resuspended in fresh Dulbecco's modified Eagle's medium before confocal fluorescence microscopy measurements were obtained.

Solid-supported bilayers comprised of DOPC and C-dot-DMPC

C-dot-DMPC-embedded small unilamellar vesicles (SUVs) composed of DOPC were prepared according to the following procedure: 100 μL of a prepared stock solution of 12.7 mM DOPC in chloroform was added to a 4 mL sample vial and then supplemented through vortexing (for ~15 min) and sonication (for 30 min) with 2 mg of C-dot-DMPC dissolved in 500 μL of chloroform. The mixture was then dried in vacuo for 12 h. The

dried lipids were hydrated in 1 mL of buffer (10 mM sodium phosphate, 100 mM sodium chloride, pH 7.4) for 1 h by occasional vortexing to completely resuspend the lipids, followed by probe sonication of the aqueous lipid mixture at room temperature in a water bath for 10 min. Then, 10 μL of 100 mM $CaCl_2$ was added to the SUV solution. Finally, glass-supported lipid bilayers were spontaneously assembled by incubating the freshly prepared SUVs on a plasma-clean coverglass surface at 25°C for 24 h. After formation of the glass-supported lipid bilayer, the unbound SUVs were gently washed off with buffer and 100% surface coverage of the supported bilayer was confirmed under the microscope. The solid-supported bilayer (SSB) was immersed in 200 μL buffer (10 mM sodium phosphate, 100 mM sodium chloride, pH 7.4) before use.

High-resolution transmission electron microscopy

High-resolution transmission electron microscopy (HRTEM) images were recorded on a 200 kV JEM-2100F transmission electron microscope (JEOL, Peabody, MA). For the HRTEM measurements, 0.5 mg of C-dots synthesized as described above were dissolved in 500 μL of chloroform, and 10 μL of the solution was placed upon an ultrathin carbon-film-coated copper grid, dried at room temperature for 2 h, and imaged.

Confocal fluorescence microscopy

Confocal microscopy images of C-dot-DMPC/DOPC GVs were acquired on an UltraVIEW system (PerkinElmer Life Sciences, Waltham, MA) equipped with an Axiovert-200 M microscope (Zeiss, Oberkochen, Germany) and a Plan-Neofluar 63×/1.4 oil objective. Excitation wavelengths of 405 nm, 440 nm, 488 nm, and 514 nm were produced by an argon/krypton laser.

Fluorescence anisotropy

SUVs were prepared by combining 39 μL of a prepared stock solution of 25.4 mM DOPC in chloroform and 2 mg of C-dot-DMPC in 200 μL of chloroform. The solution was then dried in vacuo, followed by dissolution in 1 mL buffer (10 mM NaH_2PO_4, pH 7.4) and sonication of the aqueous lipid mixture at room temperature for 10 min using a Vibra-Cell VCX130 ultrasonic cell disrupter (Sonics, Newtown, CT). Then, 360 μL of the freshly prepared SUV solution was placed in a quartz cuvette. The fluorescence emission anisotropy of the C-dot-DMPC/DOPC vesicles was measured at 463 nm before and after addition of a 40 μL solution of each compound at room temperature (excitation 375 nm) on an FL920 spectrofluorimeter (Edinburgh Instruments, Livingston, UK). Anisotropy values were automatically calculated by the spectrofluorimeter software.

Fluorescence lifetime measurements

The fluorescence lifetimes of C-dot-DMPC/DOPC SUVs before and 15 min after addition of each compound were measured using 405 nm excitation and 480 nm emission on an IBH FluoroHub TCSPC lifetime luminescence spectrophotometer fitted with a NanoLED-405L laser diode (both from HORIBA Jobin Yvon, Edison, NJ), with peak wavelength at 406 nm in the time-correlated single-photon-counting mode. Intensity decay curves were fitted as a sum of exponential terms:

$$F(t) = \sum \alpha_i \exp(-t/\tau_i),$$

where α_i represents the preexponential factor for the time-resolved decay of the component with a lifetime τ_i. The decay parameters were recovered using a nonlinear iterative fitting procedure based on the Marquardt algorithm. The quality of the fit was assessed over the entire decay, including the rising edge, and tested with other statistical parameters (e.g., the reduced χ^2 ratio). For fluorescence lifetime measurements, 900 μL solutions of SUVs consisting of C-dot-DMPC/DOPC were used and the changes in lifetime were measured after addition of 100 μL of a 1 mM solution of each compound. In the case of SUVs composed of C-dot-DMPC/DOPC, the decay curve was fitted with a multiexponential function comprising three lifetimes, and the amplitude average lifetime $<\tau>$ was calculated using the following equation:

$$\langle\tau\rangle = \frac{\alpha_1\tau_1 + \alpha_2\tau_2 + \alpha_3\tau_3}{\alpha_1 + \alpha_2 + \alpha_3}.$$

Förster resonance energy transfer

For Förster resonance energy transfer (FRET) experiments, SUVs were prepared according to the procedure indicated above. FRET experiments were carried out using 2 mg C-dot-DMPC and NBD-PE (10 μM) as a donor-acceptor pair embedded in 1 mL of SUVs composed of DOPC (1 mM). Then, 180 μL of the freshly prepared solution of 1 mM SUVs was mixed with 20 μL of a 1 mM solution of each compound. Fluorescence emission spectra ($\lambda_{ex} = 350$ nm) were acquired 15 min after addition in the range of 400−600 nm using a Varioskan 96-well plate reader (Thermo Fisher, Vantaa, Finland). The ratio F_D/F_A was calculated as a direct measure of FRET efficiency between the C-dot-DMPC donor and NBD-PE acceptor (where F_D and F_A represent the fluorescence intensity of the donor and accepter, respectively) (28). The ratio F_D/F_A was used to compare the FRET efficiency before and after the addition of each tested compound. The F_D/F_A values were normalized according to $(F_D/F_A)_0$, which corresponds to the fluorescence intensity ratio before the addition of test compounds.

FRAP

FRAP experiments were carried out at 25°C on an UltraVIEW system (PerkinElmer Life Sciences) equipped with Axiovert-200 M microscope (Zeiss) and a Plan-Neofluar 63×/1.4 oil objective. A 2.4 μm circular spot was irreversibly photobleached by a 405 nm laser for a period of 400 ms. The fluorescence intensities of the bleached circular spots and surrounding areas (used as control) were monitored over time using a 63×/1.4 oil objective. The mobile fraction (M_F) of the C-dot-DMPC embedded in either the glass-supported bilayer or GVs was measured according to the following equation:

$$M_F = \frac{I_\infty - I_0}{I_i - I_0} \times 100,$$

where I_i, I_0, and I_∞ are the total fluorescence intensities within the circular photobleached region before the bleaching pulse, immediately after bleaching, and after recovery where the fluorescence intensity reaches a plateau, respectively.

The diffusion constants were calculated according to the equation

$$D = \mathrm{w}^2/4\mathrm{t}_{1/2},$$

where w is the radius of the bleached region of interest. This equation assumes unrestricted two-dimensional diffusion in a bleached area with no recovery from above and below the focal plane. The recovery curves in the FRAP experiments were obtained 15 min after the addition of 20 μL of a 1 mM solution of each compound.

RESULTS AND DISCUSSION

Synthesis and characterization

Fig. 1 depicts a structural and optical characterization of the phospholipid/C-dot conjugates. The C-dot-labeled lipids

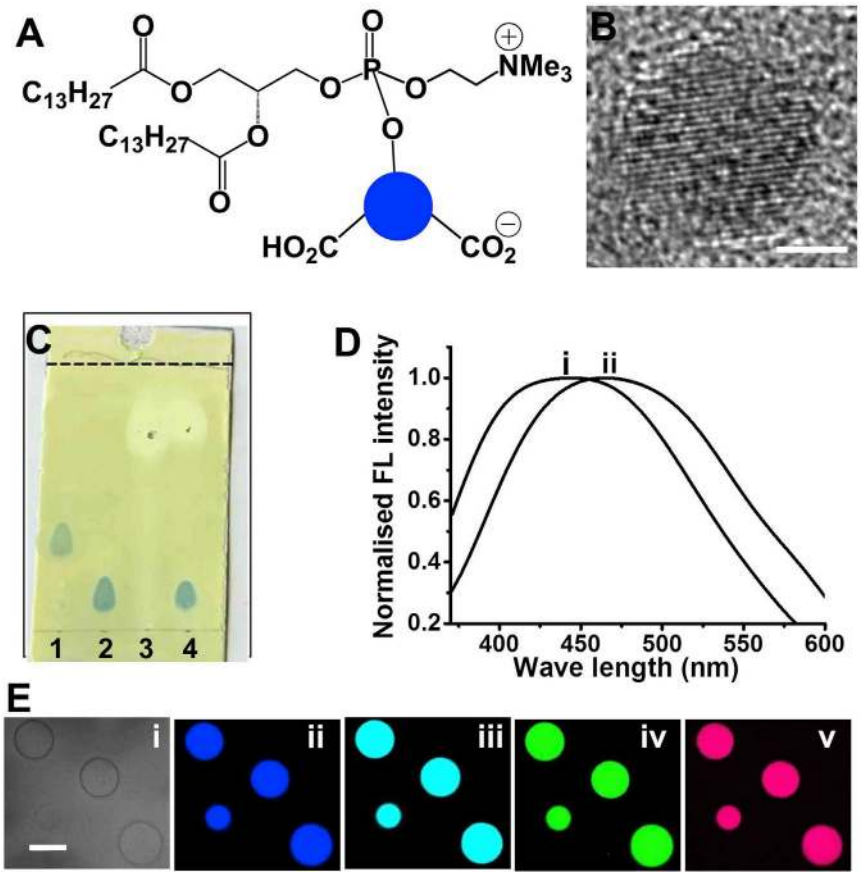

FIGURE 1 Synthesis and characterization of the C-dot-DMPC conjugate. (*A*) Chemical structure of the C-dot-DMPC molecule; the blue circle corresponds to the C-dot. (*B*) HRTEM image of a typical C-dot used in the synthesis. Scale bar, 1 nm. (*C*) Image of a TLC plate after elution, spraying with visualization reagent for detection of phosphate groups. The different columns correspond to 1) the C-dot-DMPC reaction product, 2) DMPC only, 3) C-dots only, and 4) a physical mixture of DMPC and C-dots that did not react. (*D*) Fluorescence emission spectra of the C-dots (excitation at 350 nm) before (*i*) and after (*ii*) coupling to DMPC in phosphate buffer (10 mM, pH 7.4). (*E*) Confocal microscopy images of GVs composed of DOPC (1 mM) and C-dot-DMPC (2 mg/mL). Bright-field (*i*) and confocal fluorescence microscopy images were recorded upon excitation at 405 nm, emission filter EM 445/60 (*ii*); excitation at 440 nm, emission filter EM 477/45 (*iii*); excitation at 488 nm, emission filter EM 525/50 (*iv*); and excitation at 514 nm, emission filter EM 525/50 (*v*). Scale bar, 10 μm. To see this figure in color, go online.

were prepared via a phosphorylation reaction between a chloride derivative of DMPC (a widely studied membrane lipid (29)) and C-dots that were synthesized via a hydrothermal method from 6-*O*-acylated fatty acid ester of *D*-glucose (Fig. S1) (26). Fig. 1 *B* depicts a representative HRTEM image of the C-dots, showing the crystalline structure of the graphitic core (30,31). The TLC data in Fig. 1 *C* verify the occurrence of covalent conjugation of the C-dots and DMPC. Specifically, the appearance of a luminescent spot (upon ultraviolet irradiation) that exhibits a different retention factor (R_f) compared with the pure samples of DMPC and C-dots, respectively, indicates that the reaction between the C-dots and DMPC was quantitative. The formation of pure C-dot-DMPC product was further confirmed by ^{31}P NMR (Fig. S2).

The fluorescence emission spectra (350 nm excitation) in Fig. 1 *D* reveal an experimentally significant shift of the emission peak of the C-dots coupled to DMPC in phosphate buffer (10 mM, pH 7.4) in comparison with the corresponding peak of the unbound C-dots in phosphate buffer (10 mM, pH 7.4), providing further evidence of the attachment of C-dots to the lipid molecule. Notably, the emission shift that is apparent in Fig. 1 *D* reflects a distinct chemical environment for the covalently bonded C-dots as compared with free C-dots in solution. Particularly striking are the confocal fluorescence microscopy images in Fig. 1 *E*, which show DOPC GVs coassembled with C-dot-DMPC. The distinct vesicle colors recorded using different excitation wavelengths and emission filters indicate that the C-dot-DMPC molecules were distributed uniformly within the vesicle bilayers. Furthermore, the C-dots retained their excitation-dependent fluorescence emission characteristics (i.e., multicolor emissions) while they were covalently bonded to the phospholipid.

Bilayer dynamics analyses

Figs. 2, 3, 4, and 5 illustrate the use of the new, to our knowledge, C-dot-DMPC probe for investigating bilayer dynamics and the effects of membrane-active molecules through the application of complementary fluorescence spectroscopy and microscopy techniques. Fluorescence anisotropy (Fig. 2 *A*), fluorescence lifetime (Fig. 2 *B*), and FRET (Fig. 3) experiments were carried out using SUVs comprised of DOPC (1 mM) and C-dot-DMPC (2 mg/mL). The SUVs were prepared by means of a conventional probe-sonication technique (32) and the C-dot-DMPC molecules were added to the lipid mixture before vesicle assembly.

Fig. 2 *A* demonstrates that the fluorescence anisotropy of vesicle-embedded C-dot-DMPC provides a sensitive probe

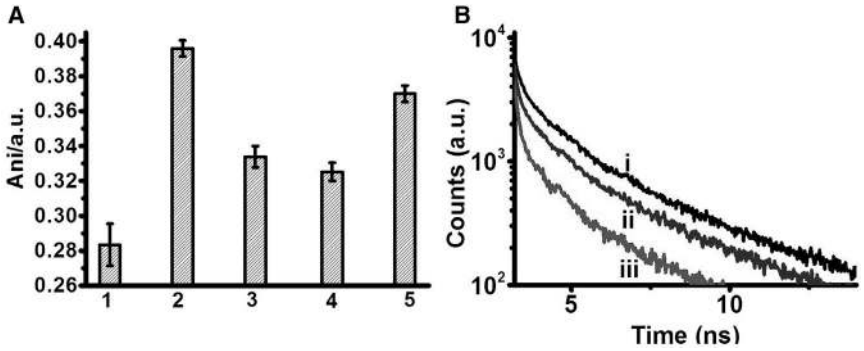

FIGURE 2 Bilayer dynamics in C-dot-DMPC/DOPC SUVs. (*A*) Fluorescence anisotropy (excitation 375 nm, emission 463 nm) of C-dot-DMPC embedded in DOPC SUVs. 1) Control C-dot-DMPC/DOPC SUVs before addition of membrane-active compounds. Anisotropy was recorded after addition of 2) PMB (0.1 mM), 3) valproic acid (0.1 mM), or 4) A$\beta_{1\text{-}40}$ (30 μM). 5) C-dot-DMPC embedded in SUVs composed of DOPC and cholesterol (7:3 mol ratio of DOPC/cholesterol). (*B*) Fluorescence lifetime decays of C-dot-DMPC embedded in the SUVs. (*i*) Control vesicles before addition of membrane-active compounds. (*ii*) C-dot-DMPC embedded in SUVs composed of DOPC and cholesterol (7:3 mol ratio of DOPC/cholesterol). (*iii*) After addition of PMB (0.1 mM) to the C-dot-DMPC/DOPC SUVs.

for assessing the effect of membrane interactions on bilayer fluidity (it should be noted that, to the best of our knowledge, this is the first time that fluorescence anisotropy of C-dots has been reported). Specifically, Fig. 2 *A* and Table S1 show that the fluorescence anisotropy of the C-dots increased upon addition to the vesicles of the widely studied membrane-active molecules polymyxin-B (PMB, an amphiphilic cytolytic peptide (33)), valproic acid (a powerful neuronal therapeutic agent (34,35)), and A$\beta_{1\text{-}40}$ (an amyloidogenic peptide that is associated with Alzheimer's disease and undergoes enhanced oligomerization upon interactions with membrane bilayers (36,37)).

Changes in the fluorescence anisotropy of bilayer-embedded dyes can be induced by modulating the lipid order parameter, providing useful insight into the lipid dynamics in membrane bilayers and the effect of membrane-interacting molecules (38,39). Indeed, the dramatic increase in fluorescence anisotropy of the C-dots after the respective additions of the three tested molecules is ascribed to their insertion into the bilayer, thereby constricting the rotational motion of the C-dot-DMPC probe. Notably, the increase of fluorescence anisotropy recorded upon addition of PMB to the vesicles (to ~0.4; Fig. 2 *A*, bar 2) is consistent with the pronounced

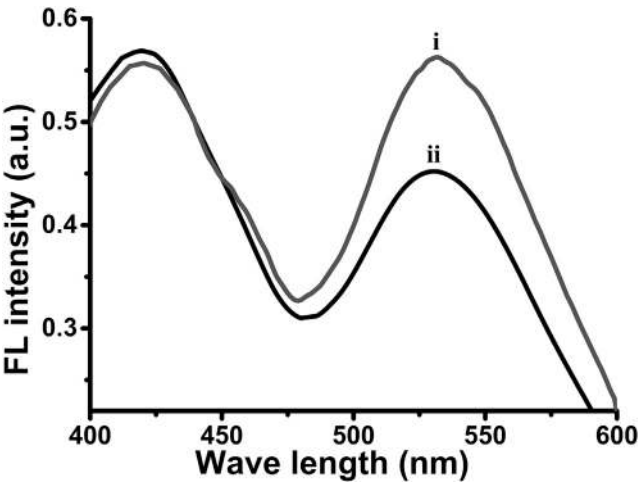

FIGURE 3 FRET experiment. Emission spectra (excitation at 350 nm) of SUVs composed of DOPC, NBD-PE (100:1 mol ratio), and C-dot-DMPC before (*i*) and after (*ii*) addition of PMB.

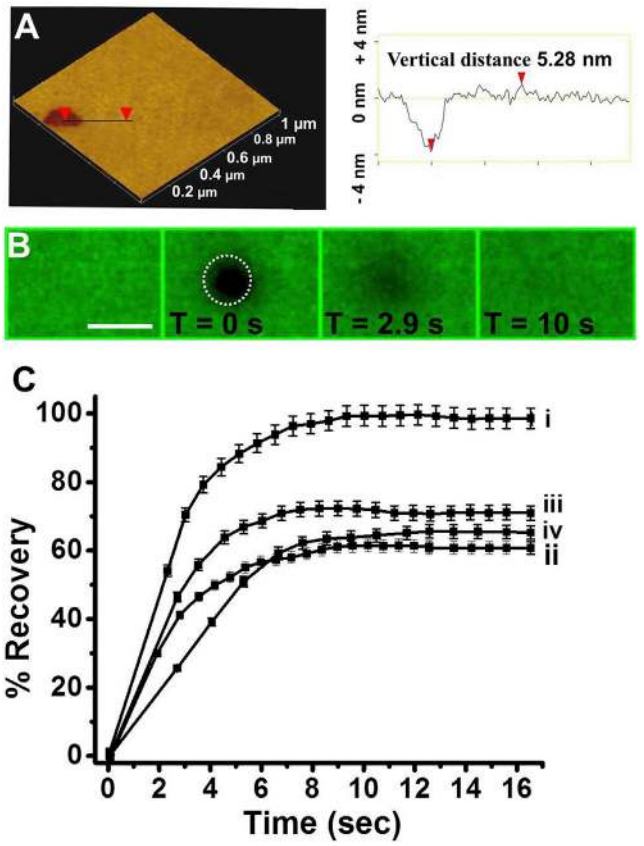

FIGURE 4 FRAP experiments in C-dot-DMPC/DOPC SSBs. (*A*) AFM image of an SSB (*left*) and the corresponding height profile (*right*). The size of the AFM image is 1 μm × 1 μm. (*B*) Confocal fluorescence microscopy images (excitation at 405 nm, emission filter EM 445/60) recorded at different times after photobleaching by a 405 nm laser (time immediately after laser irradiation is defined as $T = 0$ s). The bleached region is indicated by the circle. Scale bar, 5 μm. (*C*) Recovery curves recorded upon incubation of the SSBs with different molecules: control SSB (*i*), PMB (*ii*), valproic acid (*iii*), and A$\beta_{1\text{-}40}$ (*iv*). Each experiment was repeated five times. To see this figure in color, go online.

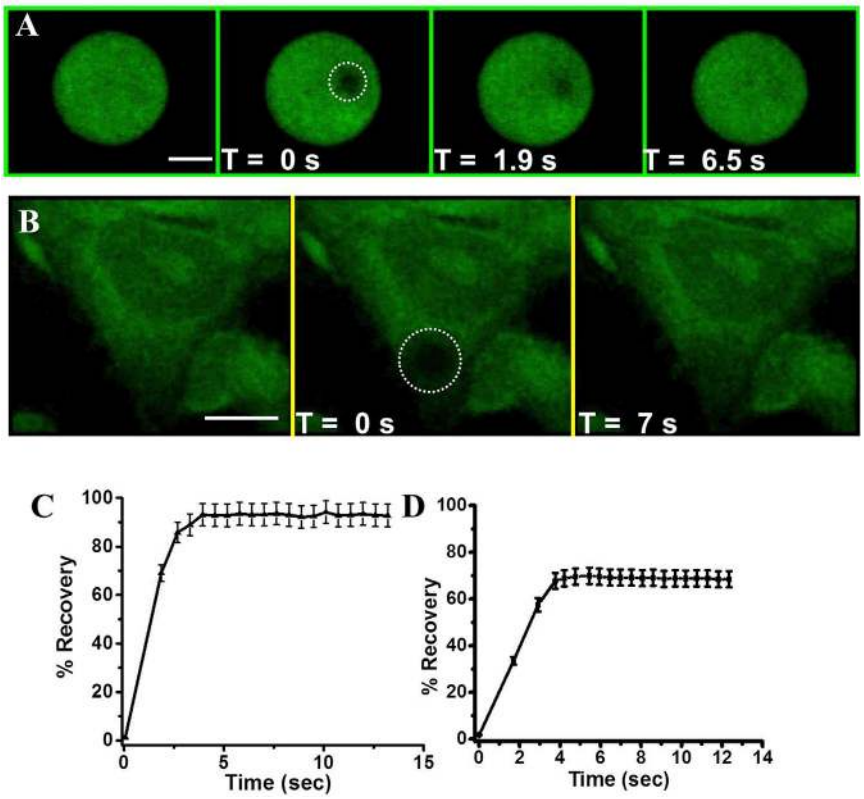

FIGURE 5 FRAP using C-dot-DMPC embedded in GVs and cell membranes. (*A* and *B*) Confocal fluorescence microscopy images (excitation at 405 nm, emission filter EM 445/60) recorded at different times after photobleaching by a 405 nm laser (time immediately after laser irradiation defined as $T = 0$ s). (*A*) C-dot-DMPC/DOPC GVs. (*B*) HeLa cells incubated with C-dot-DMPC. Scale bars, 5 μm. (*C*) Recovery curve corresponding to the FRAP experiment shown in (*A*). (*D*) Recovery curve corresponding to the FRAP experiment shown in (*B*). Each experiment was repeated five times. To see this figure in color, go online.

membrane affinity and significant bilayer reorganization induced by this peptide (40). Fig. 2 *A* also reveals that both valproic acid (Fig. 2 *A*, bar 3) and A$\beta_{1\text{-}40}$ (Fig. 2 *A*, bar 4) gave rise to decreased bilayer fluidity (as reflected in the higher fluorescence anisotropy values), consistent with membrane binding of both molecules (41,42).

To confirm that the higher fluorescence anisotropy of the C-dot-DMPC in SUVs is correlated with the extent of bilayer fluidity, we additionally recorded the anisotropy in bilayers composed of C-dot-DMPC/DOPC and also a high percentage of cholesterol (Fig. 2 *A*, bar 5). Cholesterol is known to increase rigidity in lipid bilayers (43), and indeed the recorded anisotropy of the C-dot-DMPC was significantly higher in the DOPC/cholesterol vesicles than in the control vesicles (Figs. 2 *A* and 5). Notably, the extent of anisotropy value changes apparent in Fig. 2 *A* (e.g., the dynamic range) is significantly more pronounced than the comparable anisotropy modulation observed in other widely employed dyes such as diphenylhexatriene (44).

Fluorescence lifetime measurements recorded in C-dot-DMPC/DOPC SUVs (outlined in Fig. 2 *B* and Table S1) corroborate the anisotropy results in Fig. 2 *A* and further underscore the sensitivity of the C-dot/DMPC probe to bilayer fluidity. Specifically, Fig. 2 *B* shows an experimentally significant decrease in fluorescence lifetime when PMB was added to the vesicles, from 2.9 ns in the control vesicles to 1.3 ns upon addition of PMB (Table S1). The faster lifetime decay induced by PMB is ascribed to greater bilayer rigidity (45), echoing the fluorescence anisotropy data in Fig. 2 *A*. Moreover, Fig. 2 *B* demonstrates that the fluorescence lifetime of the C-dots was similarly reduced (to 1.9 ns; Table S1) when C-dot-DMPCs were embedded within vesicles containing DOPC and 30% cholesterol (45).

The C-dots' fluorescence lifetime was also reduced, albeit to a lower extent, after addition of valproic acid or A$\beta_{1\text{-}40}$ (Table S1), consistent with the smaller effects of these molecules upon the lipid bilayers, as reflected in the fluorescence anisotropy data in Fig. 2 *A*. We believe that, similar to what has been observed for other lipid dyes, the fluorescence decay kinetics of the C-dot probe is closely related to radiative and nonradiative pathways that depend on the bilayer surface environment (46). This dependence might explain the trend we recorded in the lifetime experiment. Specifically, it is known that PMB, which exhibits cytolytic properties, induces significant reorganization upon binding of lipid bilayers (47), consistent with the pronounced decrease in fluorescence lifetime recorded in Fig. 2 *B*. On the other hand, although both valproic acid and A$\beta_{1\text{-}40}$ are membrane active, their disruption of bilayer surfaces is rather small, explaining the minimal change of fluorescence lifetime. This is also likely the scenario in the case of cholesterol; in fact, previous studies have also reported shorter lifetimes upon incorporation of cholesterol within vesicle bilayers (45).

The FRET experiment depicted in Fig. 3 further attests to the utility of the C-dot-phospholipid conjugate as a probe

for bilayer dynamics and the effects of membrane-active compounds. FRET is sensitive to slight variations in intermolecular distances between membrane-embedded fluorescent donors and acceptors, and modulations of FRET efficiency have been related to changes in bilayer fluidity and to lipid diffusion processes (48,49). The fluorescence spectra in Fig. 3 were recorded in SUVs consisting of DOPC, C-dot-DMPC as the fluorescent energy donor, and (N-(7-nitrobenz-2-oxa-1,3-diazol-4-yl)-1,2-dihexadecanoyl-*sn*-glycero-3-phosphoethanolamine) (NBD-PE) as the fluorescence acceptor. The fluorescence emission spectrum (excitation at 350 nm) of the control C-dot-DMPC/NBD-PE/DOPC vesicles features peaks at around 425 nm and 540 nm (Fig. 3, spectrum i) corresponding to the emission signals of the C-dot-DMPC and NBD-PE, respectively, and reflecting FRET from the C-dot donors to the NBD-PE acceptors.

Importantly, addition of PMB to the vesicles altered the ratio between the two peaks, reducing the intensity of the emission peak at 540 nm from NBD-PE (fluorescence acceptor; F_A) while simultaneously increasing the C-dot-DMPC emission peak at 425 nm (fluorescence donor, F_D; Fig. 3, ii). The higher value of (F_D/F_A) after PMB addition as compared with the control vesicles (($F_D/F_A)_0 = 1$) indicates a lower FRET efficiency (Table S1). The reduction of FRET is ascribed to insertion of PMB into the bilayer, restricting lipid fluidity and disrupting energy transfer between the C-dot donors and the NBD-PE acceptors (50). Changes in the $(F_D/F_A)_0$ values and hence the FRET efficiencies induced by addition of valproic acid and A$\beta_{1\text{-}40}$ are outlined in Table S1.

Figs. 4 and 5 depict the application of FRAP experiments utilizing the C-dot-phospholipid conjugate as the fluorescent probe. FRAP is a powerful technique for probing membrane fluidity (51), diffusion processes in membranes (8), modulation of lipid dynamics by membrane proteins (52), ligand-receptor binding (53,54), and bilayer interactions of membrane-active molecules (55,56). Fig. 4 presents FRAP analyses of SSBs composed of 1 mM DOPC and C-dot-DMPC (2 mg/mL). SSBs have been widely used as model membranes in FRAP experiments; however, attaining bilayer integrity and fluorescent dye distribution in the supported bilayers is considered a major challenge (57). Fig. 4 *A* displays an atomic force microscopy (AFM) image and corresponding height profile of the C-dot-DMPC/DOPC SSBs, demonstrating a highly uniform morphology and bilayer thickness, and confirming that the embedded C-dot-DMPC probe did not adversely affect bilayer organization.

The confocal fluorescence microscopy images in Fig. 4 *B* illustrate the progression of a FRAP experiment carried out using C-dot-DMPC as the fluorescent probe within the SSB. After an intense laser irradiation at 405 nm (duration of 400 ms), the C-dot fluorescence was irreversibly photobleached, producing a circular black region within the fluorescent SSB (Fig. 4 *B*). The fluorescence in the photobleached region gradually recovered due to lateral lipid diffusion (8) and reached a fluorescence emission close to the initial value after ~10 s (Fig. 4 *B*).

Fig. 4 *C* depicts FRAP recovery curves that were recorded after addition of PMB, valproic acid, or A$\beta_{1\text{-}40}$ to the SSBs. The diffusion constants and percentages of mobile fraction of the dye in SSBs extracted from the recovery curves (11) are summarized in Table 1. Importantly, the percentage of mobile C-dot-DMPC fluorophore in the control SSB was ~99% (Table 1). This result signifies that the fluorescent C-dot-DMPC conjugate is mobile within the two-dimensional plane of the bilayer (58), and further supports homogeneous internalization of C-dot-DMPC into the SSB without the formation of microscopic patches or defects. The lateral diffusion constant (D) for the DOPC bilayer was 1.7×10^{-9} cm^2s^{-1} (9).

The recovery curves in Fig. 4 *C* and corresponding dynamic parameters in Table 1 highlight the distinct effects of the three compounds examined. Specifically, PMB, valproic acid, and A$\beta_{1\text{-}40}$ all reduced the percentage of mobile fraction compared with the control SSBs. This result indicates a lower homogeneity in the SSBs, which is ascribed to the formation of lipid patches upon insertion of the membrane-active species (59,60). Interestingly, as depicted in Table 1, A$\beta_{1\text{-}40}$ also induced a significant decrease of the lateral diffusion constant (~50%) as compared with the control SSBs. The reduced diffusion combined with the low percentage of mobile fraction (66%; Table 1) is indicative of a significant restriction of lateral mobility and membrane fluidity induced by A$\beta_{1\text{-}40}$. This result is ascribed to bilayer interactions and membrane-associated aggregation of this amyloidogenic peptide, giving rise to lower bilayer fluidity and inhibited lipid mobility (51,61).

In contrast to A$\beta_{1\text{-}40}$, PMB and valproic acid did not significantly alter the lateral diffusion coefficient of the C-dot-DMPC probe (Table 1). The insignificant difference in lateral diffusion constants compared with the control DOPC SSBs likely corresponds to the fact that FRAP generally provides information about processes occurring on a macroscopic scale rather than on a molecular level (62). Specifically, since FRAP illuminates the average mobility of a relatively large number of bilayer-embedded fluorescent molecules, the technique exhibits less sensitivity to the effects of faster-diffusing molecules such as PMB and valproic acid.

TABLE 1 FRAP Parameters Extracted from the Recovery Curves in Fig. 4 *C*

	D [10^{-9} cm^2s^{-1}][a]	M_F (%)[b]
Control C-dot-DMPC/DOPC SSB	1.7 ± 0.2	99 ± 3
PMB	1.5 ± 0.2	61 ± 5
Valproic acid	1.7 ± 0.3	72 ± 2
A$\beta_{1\text{-}40}$	0.7 ± 0.3	66 ± 4

[a]Lateral diffusion constant (58).
[b]Percentage of mobile fraction (58,60).

Although the majority of FRAP studies have been performed in SSB configurations, applications of FRAP in vesicular lipid systems (1,8) and in actual cell membrane environments (9) are important because they provide comprehensive information about lipid diffusion in membranes. Accordingly, we carried out FRAP experiments using the new, to our knowledge, C-dot-phospholipid conjugate in GVs and in membranes of actual cells (Fig. 5). Fig. 5 depicts confocal fluorescence microscopy images of C-dot-DMPC/DOPC GVs (Fig. 5 *A*) and HeLa cells incubated with C-dot-DMPC (Fig. 5 *B*) that were recorded at different times after photobleaching. Also shown are the corresponding recovery curves (Fig. 5, *C* and *D*). The FRAP data in Fig. 5 demonstrate effective photobleaching and recovery of the C-dot fluorescence in both membrane systems, yielding diffusion constants of $D = 2.9 \pm 0.2 \times 10^{-9}$ cm^2s^{-1} in the GVs and $D = 2 \pm 0.3 \times 10^{-9}$ cm^2s^{-1} in the HeLa cell membranes. It should be noted that staining the HeLa cells with C-dot-DMPC (e.g., Fig. 5 *B*) minimally affected cell viability (Fig. S3).

DISCUSSION

Here, we have introduced a new, to our knowledge, probe for membrane environments and processes based upon conjugation of C-dots and phospholipids. The unique properties of C-dots (specifically, their broad excitation/emission range, brightness, optical and chemical stability, and biocompatibility) make the C-dot-lipid conjugate a sensitive platform for analysis of membrane dynamics and the impact of membrane-active molecules.

The advantages of the C-dot-phospholipid conjugates over existing lipid dyes are important aspects of this work. The main advantages of the new, to our knowledge, C-dot-phospholipid conjugates are as follows:

Multifunctionality: In contrast to conventional fluorescent probes such as rhodamine and fluorescein, the C-dot-phospholipid probe can provide imaging capabilities, fluorescence anisotropy, and sensitivity of the fluorescence signal to the molecular environment (i.e., polarity, hydrophobicity), as well as FRAP and FRET properties.

Broad excitation/emission range: The wide excitation/emission range of C-dot-phospholipid conjugates is significant for both fundamental biophysical and practical reasons. Specifically, it allows the use of the C-dot conjugate as a versatile donor or acceptor in FRET experiments. Furthermore, this feature means that multicolor fluorescence imaging experiments can be carried out, and applications of the new, to our knowledge, probe are not limited by available excitation wavelengths. Fig. S4 provides a pertinent example of a two-color confocal microscopy imaging experiment applied using the C-dot-DMPC probe.

Versatile synthesis pathways: C-dots can be easily prepared from a broad variety of carbon-containing building blocks. This is important since the choice of the carbonaceous reagents used shapes the photophysical properties of the resultant C-dots (excitation/emission range, quantum yield, etc.). In addition, coupling of the C-dots can be readily carried out with different lipid molecules.

Biocompatibility: C-dots are more biocompatible than many fluorescent dyes, particularly popular probes such as inorganic quantum dots, thus pointing to a possible use of C-dot-lipids as generic dyes for cellular processes in addition to their application as membrane probes.

Before the C-dot-phospholipid conjugate technology can achieve broad applicability, it must overcome several hurdles. A low quantum yield and insufficient brightness could be encountered, limiting the use of the new, to our knowledge, fluorescent probes for cell studies. Moreover, high concentrations of the C-dot-phospholipid probes (possibly used to enhance fluorescence signals) might adversely affect cell viability.

CONCLUSIONS

We have constructed a new, to our knowledge, fluorescent probe for membrane dynamics by coupling a carbon dot to a phospholipid. The C-dot-phospholipid conjugate readily inserted into biomimetic and actual membranes, allowing the application of various biophysical techniques, including fluorescence anisotropy, fluorescence lifetime, FRET, and FRAP for studying lipid mobility, bilayer fluidity, and lateral diffusion processes in membrane bilayers. Specifically, we employed the C-dot-phospholipid probe to analyze the membrane interactions of PMB, valproic acid, and $A\beta_{1\text{-}40}$, and obtained highly sensitive information about the influence of these molecules on dynamical parameters pertaining to lipid bilayers. In particular, the experiments revealed the significant effect of PMB bilayer interactions and the consequence of $A\beta_{1\text{-}40}$ membrane-induced aggregation for lateral lipid diffusion. The C-dot/lipid conjugate is a versatile tool for membrane studies, expanding fluorescence-based studies of membrane dynamics.

SUPPORTING MATERIAL

Four figures and one table are available at http://www.biophysj.org/biophysj/supplemental/S0006-3495(16)30157-6.

AUTHOR CONTRIBUTIONS

S.N. planned and conducted the experiments, and contributed to writing of the manuscript. R.M. and S.K.B. contributed to sample preparation and analysis. S.K. and J.J. contributed technical analysis. R.J. directed the research and wrote the manuscript.

ACKNOWLEDGMENTS

We are grateful to Manoj Kumar Pal (Department of Life Sciences, Ben-Gurion University of the Negev) for help with the FRAP experiments and Gilad Haran and Haim Aviram (Department of Chemical Physics, Weizmann Institute of Science) for help with fluorescence lifetime measurements. We also thank Avijit Paul, Tasleem Arif, and Varda Shoshan-Barmatz (Department of Life Sciences, Ben-Gurion University of the Negev), and Oshrit Ben David and Eyal Arbely (Department of Chemistry and The National Institute for Biotechnology in the Negev, Ben-Gurion University of the Negev) for help with cell imaging experiments.

This work was supported by the Kreitman School of Advanced Graduate Studies at Ben Gurion University (S.N.).

REFERENCES

1. Pucadyil, T. J., S. Mukherjee, and A. Chattopadhyay. 2007. Organization and dynamics of NBD-labeled lipids in membranes analyzed by fluorescence recovery after photobleaching. *J. Phys. Chem. B.* 111:1975–1983.
2. Guo, L., J. Y. Har, …, T. Wohland. 2008. Molecular diffusion measurement in lipid bilayers over wide concentration ranges: a comparative study. *ChemPhysChem.* 9:721–728.
3. Tero, R. 2012. Substrate effects on the formation process, structure and physicochemical properties of supported lipid bilayers. *Materials (Basel).* 5:2658.
4. Singer, S. J., and G. L. Nicolson. 1972. The fluid mosaic model of the structure of cell membranes. *Science.* 175:720–731.
5. Ma, Y., R. Jiang, …, X.-L. Sun. 2012. Chemoselectively surface funtionalizable tethered bilayer lipid membrane for versatile membrane mimetic systems fabrication. *J. Mater. Chem.* 22:6148–6155.
6. Simons, K., and E. Ikonen. 1997. Functional rafts in cell membranes. *Nature.* 387:569–572.
7. Engelman, D. M. 2005. Membranes are more mosaic than fluid. *Nature.* 438:578–580.
8. Macháň, R., and M. Hof. 2010. Lipid diffusion in planar membranes investigated by fluorescence correlation spectroscopy. *Biochim. Biophys. Acta.* 1798:1377–1391.
9. Ladha, S., A. R. Mackie, and D. C. Clark. 1994. Cheek cell membrane fluidity measured by fluorescence recovery after photobleaching and steady-state fluorescence anisotropy. *J. Membr. Biol.* 142:223–228.
10. Metcalf, T. N., J. L. Wang, and M. Schindler. 1986. Lateral diffusion of phospholipids in the plasma membrane of soybean protoplasts: evidence for membrane lipid domains. *Proc. Natl. Acad. Sci. USA.* 83:95–99.
11. Ladha, S., A. R. Mackie, …, H. Duclohier. 1996. Lateral diffusion in planar lipid bilayers: a fluorescence recovery after photobleaching investigation of its modulation by lipid composition, cholesterol, or alamethicin content and divalent cations. *Biophys. J.* 71:1364–1373.
12. Baker, S. N., and G. A. Baker. 2010. Luminescent carbon nanodots: emergent nanolights. *Angew. Chem. Int. Ed. Engl.* 49:6726–6744.
13. Shen, J., Y. Zhu, …, C. Li. 2012. Graphene quantum dots: emergent nanolights for bioimaging, sensors, catalysis and photovoltaic devices. *Chem. Commun. (Camb.).* 48:3686–3699.
14. Cao, L., X. Wang, …, Y.-P. Sun. 2007. Carbon dots for multiphoton bioimaging. *J. Am. Chem. Soc.* 129:11318–11319.
15. Li, H., Z. Kang, …, S.-T. Lee. 2012. Carbon nanodots: synthesis, properties and applications. *J. Mater. Chem.* 22:24230–24253.
16. Michalet, X., F. F. Pinaud, …, S. Weiss. 2005. Quantum dots for live cells, in vivo imaging, and diagnostics. *Science.* 307:538–544.
17. Choi, S., R. M. Dickson, and J. Yu. 2012. Developing luminescent silver nanodots for biological applications. *Chem. Soc. Rev.* 41:1867–1891.
18. Yang, S.-T., L. Cao, …, Y.-P. Sun. 2009. Carbon dots for optical imaging in vivo. *J. Am. Chem. Soc.* 131:11308–11309.
19. Liu, R., D. Wu, …, Q. Li. 2009. An aqueous route to multicolor photoluminescent carbon dots using silica spheres as carriers. *Angew. Chem. Int. Ed. Engl.* 48:4598–4601.
20. Cao, L., M. J. Meziani, …, Y.-P. Sun. 2013. Photoluminescence properties of graphene versus other carbon nanomaterials. *Acc. Chem. Res.* 46:171–180.
21. Xu, Y., M. Wu, …, Y.-K. Zhang. 2013. Nitrogen-doped carbon dots: a facile and general preparation method, photoluminescence investigation, and imaging applications. *Chemistry.* 19:2276–2283.
22. Yang, Z.-C., M. Wang, …, J. Wang. 2011. Intrinsically fluorescent carbon dots with tunable emission derived from hydrothermal treatment of glucose in the presence of monopotassium phosphate. *Chem. Commun. (Camb.).* 47:11615–11617.
23. Fowley, C., B. McCaughan, …, J. F. Callan. 2012. Highly luminescent biocompatible carbon quantum dots by encapsulation with an amphiphilic polymer. *Chem. Commun. (Camb.).* 48:9361–9363.
24. Jaiswal, A., S. S. Ghosh, and A. Chattopadhyay. 2012. One step synthesis of C-dots by microwave mediated caramelization of poly(ethylene glycol). *Chem. Commun. (Camb.).* 48:407–409.
25. Roy, S., B. Korzeniowska, …, C. McDonagh. 2015. Biocompatibility and bioimaging application of carbon nanoparticles synthesized by phosphorus pentoxide combustion method. *J. Nanomater.* 2015:1–10.
26. Nandi, S., R. Malishev, …, R. Jelinek. 2014. Membrane analysis with amphiphilic carbon dots. *Chem. Commun. (Camb.).* 50:10299–10302.
27. Moscho, A., O. Orwar, …, R. N. Zare. 1996. Rapid preparation of giant unilamellar vesicles. *Proc. Natl. Acad. Sci. USA.* 93:11443–11447.
28. Shi, L., N. Rosenzweig, and Z. Rosenzweig. 2007. Luminescent quantum dots fluorescence resonance energy transfer-based probes for enzymatic activity and enzyme inhibitors. *Anal. Chem.* 79:208–214.
29. Marquardt, D., J. A. Williams, …, T. A. Harroun. 2014. Dimyristoyl phosphatidylcholine: a remarkable exception to α-tocopherol's membrane presence. *J. Am. Chem. Soc.* 136:203–210.
30. Tang, L., R. Ji, …, S. P. Lau. 2012. Deep ultraviolet photoluminescence of water-soluble self-passivated graphene quantum dots. *ACS Nano.* 6:5102–5110.
31. Kwon, W., and S.-W. Rhee. 2012. Facile synthesis of graphitic carbon quantum dots with size tunability and uniformity using reverse micelles. *Chem. Commun. (Camb.).* 48:5256–5258.
32. Ding, H., J. A. Schauerte, D. G. Steel, and A. Gafni. 2012. β-Amyloid (1–40) peptide interactions with supported phospholipid membranes: a single-molecule study. *Biophys. J.* 103:1500–1509.
33. Raynor, R. L., B. Zheng, and J. F. Kuo. 1991. Membrane interactions of amphiphilic polypeptides mastoparan, melittin, polymyxin B, and cardiotoxin. Differential inhibition of protein kinase C, Ca2+/calmodulin-dependent protein kinase II and synaptosomal membrane Na,K-ATPase, and Na+ pump and differentiation of HL60 cells. *J. Biol. Chem.* 266:2753–2758.
34. Brunn, J., V. Wiroth, …, M. Sabolek. 2014. Valproic acid in normal therapeutic concentration has no neuroprotective or differentiation influencing effects on long term expanded murine neural stem cells. *Epilepsy Res.* 108:623–633.
35. Chiu, C.-T., Z. Wang, …, D.-M. Chuang. 2013. Therapeutic potential of mood stabilizers lithium and valproic acid: beyond bipolar disorder. *Pharmacol. Rev.* 65:105–142.
36. Dürr, U. H. N., M. Gildenberg, and A. Ramamoorthy. 2012. The magic of bicelles lights up membrane protein structure. *Chem. Rev.* 112:6054–6074.
37. Kotler, S. A., P. Walsh, …, A. Ramamoorthy. 2014. Differences between amyloid-β aggregation in solution and on the membrane: insights into elucidation of the mechanistic details of Alzheimer's disease. *Chem. Soc. Rev.* 43:6692–6700.
38. Yengo, C. M., and C. L. Berger. 2010. Fluorescence anisotropy and resonance energy transfer: powerful tools for measuring real time protein dynamics in a physiological environment. *Curr. Opin. Pharmacol.* 10:731–737.

39. Gradinaru, C. C., D. O. Marushchak, …, U. J. Krull. 2010. Fluorescence anisotropy: from single molecules to live cells. *Analyst (Lond.).* 135:452–459.

40. Clausell, A., M. Pujol, …, Y. Cajal. 2003. Influence of polymyxins on the structural dynamics of Escherichia coli lipid membranes. *Talanta.* 60:225–234.

41. Kremer, J. J., M. M. Pallitto, …, R. M. Murphy. 2000. Correlation of β-amyloid aggregate size and hydrophobicity with decreased bilayer fluidity of model membranes. *Biochemistry.* 39:10309–10318.

42. Tangorra, A., G. Curatola, and E. Bertoli. 1991. Evaluation of antiepileptic drug effect on membrane fluidity. *Exp. Mol. Pathol.* 55:180–189.

43. Cooper, R. A. 1978. Influence of increased membrane cholesterol on membrane fluidity and cell function in human red blood cells. *J. Supramol. Struct.* 8:413–430.

44. Illinger, D., G. Duportail, …, J.-G. Kuhry. 1995. A comparison of the fluorescence properties of TMA-DPH as a probe for plasma membrane and for endocytic membrane. *Biochim. Biophys. Acta.* 1239:58–66.

45. de Almeida, R. F. M., J. Borst, …, A. J. W. G. Visser. 2007. Complexity of lipid domains and rafts in giant unilamellar vesicles revealed by combining imaging and microscopic and macroscopic time-resolved fluorescence. *Biophys. J.* 93:539–553.

46. Orte, A., J. M. Alvarez-Pez, and M. J. Ruedas-Rama. 2013. Fluorescence lifetime imaging microscopy for the detection of intracellular pH with quantum dot nanosensors. *ACS Nano.* 7:6387–6395.

47. Katz, M., H. Tsubery, …, R. Jelinek. 2003. Lipid binding and membrane penetration of polymyxin B derivatives studied in a biomimetic vesicle system. *Biochem. J.* 375:405–413.

48. Ghatak, C., V. G. Rao, …, N. Sarkar. 2011. The effect of membrane fluidity on FRET parameters: an energy transfer study inside small unilamellar vesicle. *Phys. Chem. Chem. Phys.* 13:3711–3720.

49. Sezgin, E., and P. Schwille. 2011. Fluorescence techniques to study lipid dynamics. *Cold Spring Harb. Perspect. Biol.* 3:a009803.

50. Chachisvilis, M., Y.-L. Zhang, and J. A. Frangos. 2006. G protein-coupled receptors sense fluid shear stress in endothelial cells. *Proc. Natl. Acad. Sci. USA.* 103:15463–15468.

51. Sasahara, K., K. Morigaki, and K. Shinya. 2013. Effects of membrane interaction and aggregation of amyloid β-peptide on lipid mobility and membrane domain structure. *Phys. Chem. Chem. Phys.* 15:8929–8939.

52. Sheetz, M. P., M. Schindler, and D. E. Koppel. 1980. Lateral mobility of integral membrane proteins is increased in spherocytic erythrocytes. *Nature.* 285:510–511.

53. Dutta, D., A. Pulsipher, …, M. N. Yousaf. 2014. PI3 kinase enzymology on fluid lipid bilayers. *Analyst (Lond.).* 139:5127–5133.

54. Tolentino, T. P., J. Wu, …, C. Zhu. 2008. Measuring diffusion and binding kinetics by contact area FRAP. *Biophys. J.* 95:920–930.

55. Reits, E. A. J., and J. J. Neefjes. 2001. From fixed to FRAP: measuring protein mobility and activity in living cells. *Nat. Cell Biol.* 3:E145–E147.

56. Fritzsche, M., and G. Charras. 2015. Dissecting protein reaction dynamics in living cells by fluorescence recovery after photobleaching. *Nat. Protoc.* 10:660–680.

57. Cruz, A., L. Vázquez, …, J. Pérez-Gil. 2005. Influence of a fluorescent probe on the nanostructure of phospholipid membranes: dipalmitoylphosphatidylcholine interfacial monolayers. *Langmuir.* 21:5349–5355.

58. Hamai, C., T. Yang, …, S. M. Musser. 2006. Effect of average phospholipid curvature on supported bilayer formation on glass by vesicle fusion. *Biophys. J.* 90:1241–1248.

59. Mc Kiernan, A. E., R. I. MacDonald, …, D. Axelrod. 1997. Cytoskeletal protein binding kinetics at planar phospholipid membranes. *Biophys. J.* 73:1987–1998.

60. Weinman, E. J., D. Steplock, …, M. Donowitz. 2009. PTH transiently increases the percent mobile fraction of Npt2a in OK cells as determined by FRAP. *Am. J. Physiol. Renal Physiol.* 297:F1560–F1565.

61. Castanho, M. A. R. B. 2010. Chiral molecular imprinting as a tool for drug sensing. *In* Membrane-Active Peptides: Methods and Results on Structure and Function. M. A. R. B. Castanho, editor. International University Line, La Jolla, CA, p. 237.

62. Waharte, F., K. Steenkeste, …, M.-P. Fontaine-Aupart. 2010. Diffusion measurements inside biofilms by image-based fluorescence recovery after photobleaching (FRAP) analysis with a commercial confocal laser scanning microscope. *Appl. Environ. Microbiol.* 76:5860–5869.